

Article

High-Temperature Compressive Properties of TiB-Reinforced Ti Alloy via In Situ Synthesis

Jing Zeng, Liping Liu, Jiazhi Yuan and Hua Chen *

School of Material Science and Engineering, Changchun University of Technology, Changchun 130012, China; m18584321309@163.com (J.Z.); look_see@163.com (L.L.); m13944910762@163.com (J.Y.)

* Correspondence: chenhua@ccut.edu.cn; Tel.: +86-431-8571-6421

Received: 9 March 2018; Accepted: 25 April 2018; Published: 27 April 2018



Abstract: In this investigation, in situ synthesis of TiB-reinforced Ti-based alloy was carried out by powder metallurgy. The Ti (TiH₂)—Al and B powders were ball milled for 40 h to obtain a mixed powder with a nominal composition of Ti-7Al-0.2B (wt. %) and TiH₂-7Al-0.2B (wt. %). After milling the mixed powder by using a vacuum hot pressing sintering furnace (1200 °C sintering temperature, 30 MPa pressure, 1 h holding pressure), TiB-reinforced Ti-based alloy was prepared in situ. The compression tests were carried out on a WDW-200 universal testing machine at 550 °C, 600 °C, and 650 °C, and at the strain rates of $1 \times 10^{-4} \text{ s}^{-1}$, $3 \times 10^{-4} \text{ s}^{-1}$, and $5 \times 10^{-4} \text{ s}^{-1}$ to investigate the alloy compression and rheological behavior of the prepared alloy. It was observed that Ti-7Al-0.2B and TiH₂-7Al-0.2B alloy formed a TiB phase and α -Ti duplex structure after low-energy ball milling and hot pressed sintering. This is because the in situ synthesis of TiB fiber reinforced phase hinders grain boundary migration and grain growth. Therefore, the TiB phase in Ti-7Al-0.2B alloy is fine, evenly distributed and effective in suppressing grain growth. Alloy materials are heat sensitive and strain-rate sensitive alloys, and the peaks of high-temperature compressive stress decrease with the decrease of the strain rate and the increase of the temperature. At the same temperature and rate conditions, the highest peak flow stress of TiH₂-7Al-0.2B is slightly higher than that of Ti-7Al-0.2B. In the ball milling and sintering process of TiH₂-7Al-0.2B alloy, the decomposition of H from TiH₂ cleanses the surface of Ti particles. This leads to the reduction of the possibility of contamination, and also has a good effect in improving the compression performance.

Keywords: in situ synthesis; TiB whisker; α -Ti alloy; high-temperature compression

1. Introduction

Ti-based composites have a range of excellent properties such as high temperature resistance, corrosion resistance, high specific strength, high specific modulus and excellent high temperature creep resistance, oxidation resistance, high thermal stability, and thermal fatigue strength [1], while the common Ti alloys do not possess these unique properties. Owing to these, the Ti-based composite materials have become unique in the field of aerospace and show potential in the development of structural materials [2].

The hot workability of Ti-based composites was determined by the microstructure of Ti matrices and distribution of reinforcements [3]. Gorsse et al. [4] found out TiB has better chemical stability, less residual stresses, and higher stiffness, as compared with other reinforcing phases such as Ti₅Si₃, CrB, B₄C, and SiC. Therefore, TiB can be considered as the best reinforcement for Ti matrices. In situ synthesis of Ti-based composites could be carried out by powder metallurgy, where the resulting TiB reinforcements do not have any interfacial reaction with the Ti matrix, and the interface is clean and has a strong binding force [5–8]. This synthesis method has become the trend of research in recent years. The size and morphology of the reinforcing phase in the composites and its distribution in the

matrix have a great influence on the properties of the generated composites. Therefore, studies on the formation mechanism of reinforcements and its influence on the properties of composite materials are of great significance for the development of high performance Ti-based composites.

The particle-reinforcing phase in the in situ synthesis of Ti-based composite materials have high strength, high hardness, and other improved characteristics. Compared to the Ti alloy matrix, the strength and elastic modulus of Ti-based composites are significantly improved. However, the existence of the particle-reinforcing phase enhances the Ti-based composites, while also lacerating the continuity of Ti alloy substrate, making it in the process of plastic deformation and showing inhomogeneity. Different from the non-reinforced Ti alloy substrate, the plastic deformation of reinforced Ti alloy substrate is a gradual process from the local to the whole. The result is that the plasticity of Ti-based composites is not only related to the plasticity of the matrix but also related to the plastic deformation of the matrix and reinforcing phases. Therefore, the strength of Ti-based composites is significantly improved while the elongation declines. In this case, the mechanical properties of Ti-based composite materials, with the same volume content as the reinforcing phase but using different processing method, could be very different [9].

Powder metallurgy is the ideal process for preparing low-cost Ti alloys [10,11]. In the preparation of Ti alloy, TiH₂ powder is commonly used instead of Ti powder. This is because the price of TiH₂ powder is lower than that of Ti powder, and TiH₂ powder can generate reversible alloying of H [12]. In the sintering process, the decomposition of TiH₂ releases H which cleans the surface of Ti powder particles. So, the possibility of Ti alloy being polluted in the production process is also reduced. In this manner, the performance of the material had been improved [13–16].

In this study, Ti-7Al alloy (α -Ti alloy) was used as the matrix of the composite material, and an in situ synthesis of TiB-reinforced Ti alloy was carried out using powder metallurgy. The major focus of this study is the preparation of TiB by using TiH₂ powder instead of Ti powder, and comparing the differences between them, as well as studying their high-temperature compression properties. The compressive deformation of the composite material could well characterize the plastic deformation behavior of the material, hence providing valuable and practical insights to the deformation and strengthening mechanisms of the composite.

2. Materials and Methods

Ti (TiH₂) powder, B powder, and Al powder were mixed and formulated into the nominal composition of the alloy with Ti-7Al-0.2B (wt. %) and TiH₂-7Al-0.2B (wt. %). The supplier of Ti, Al, B, and TiH₂ powders is the General Research Institute for Nonferrous Metals (Beijing, China). The purity of Ti, TiH₂, and B powders are greater than 99.5%, and the purity of Al powder is 99.9%. The size of Ti powder, B powder, Al powder, and TiH₂ powder are 25 μ m, 5 μ m, 75 μ m, and 75 μ m, respectively.

Horizontal planetary ball mill (NJ1-QM-ISP04, Beijing and KTG Yuanda science and Technology Ltd., Beijing, China) was used for low energy ball milling with a 10:1 ball-to-powder mass ratio and speed of 160 r/min for 40 h. The mixed powder was vacuum hot-pressed sintered by vacuum hot pressing sintering furnace (ZT-40-20-type, Shanghai Chenhua Electric Furnace Limited Company, Shanghai, China) with 1200 °C of sintering temperature, and 30 MPa pressure. Heat preservation and keep pressure were 1 h. After the furnace cooling, the sintered structure is the organization of α -Ti with less than 500 nm and fine TiB phase. The sintered alloy rod was cut into a compressed sample of Φ 6 mm \times 9 mm (Chinese Standard GB/T 7314).

Compression tests were performed on a universal testing machine (DDL50, CIMACH, Changchun, China). The deformation temperature was 550 °C, 600 °C, and 650 °C, the strain rate was $1 \times 10^{-4} \text{ s}^{-1}$, $3 \times 10^{-4} \text{ s}^{-1}$, and $5 \times 10^{-4} \text{ s}^{-1}$, and compression deformation was 40%. Because the sample was prone to cracking at 550 °C, the amount of compressive deformation was set to 30% at 550 °C. In order to obtain the organization of high-temperature compression, the sample was cooled by quench after the compression was completed.

The phase composition analysis of sintered samples was carried out using a X-ray diffractometer (XRD, D/MAX-2000PC, Rigaku, Beijing, China). The microstructure was analyzed by Scanning electron microscopy (SEM, JSM-5500LV, JEOL Ltd., Tokyo, Japan), Transmission electron microscopy (TEM, JEM-2000EX, JEOL Ltd., Tokyo, Japan), and High resolution transmission electron microscopy (HRTEM, FEI- Talos F20 S, FEI Technologies Inc., Beaverton, OR, USA).

3. Results

3.1. Status of the Ball Milling Powders

Figure 1 shows the SEM images of milled powders. Specifically, Figure 1a,c are images of the low energy ball milling of Ti-7Al-0.2B for 5 h and 40 h, respectively, whereas Figure 1b,d are the images of low energy ball milling of TiH₂-7Al-0.2B for 5 h and 40 h, respectively. Compared with ball milling for 5 h, Ti-7Al-0.2B, and TiH₂-7Al-0.2B powder obtained after ball milling for 40 h shows a certain degree of refinement, where the size of most of the particles is reduced to 10 μm and 5 μm, respectively. It can be observed that the shape of large particles in Ti-7Al-0.2B is equiaxed, and the corners of powder particles become dull. As the impact of the low energy ball mill is small, the larger powder particles cannot be broken. In contrast, the large powder particles can be broken in the thin and regular edges. This is due to the action of centrifugal force, and the continuous extrusion of the grinding ball and its impact on the powder particles. Hence, the edge of the powder particles is blunted. After milling for 40 h, the particle breakage of the TiH₂-7Al-0.2B composite powder is more obvious than that of Ti-7Al-0.2B, and the effect of powder refining is better. This is mainly due to the higher brittleness of TiH₂ powder [17], so the refinement effect of TiH₂-7Al-0.2B is more obvious in the ball milling process.

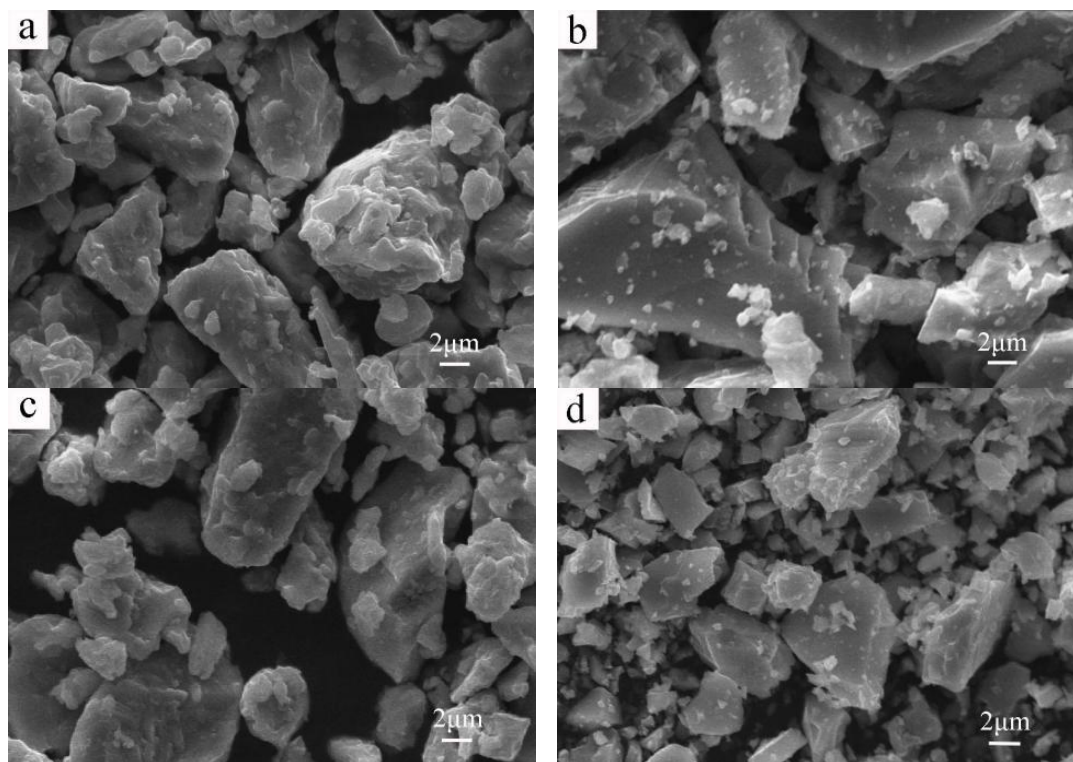


Figure 1. Micrograph of composite powders: (a) Ti-7Al-0.2B ball milling 5 h; (b) TiH₂-7Al-0.2B ball milling 5 h; (c) Ti-7Al-0.2B ball milling 40 h; (d) TiH₂-7Al-0.2B ball milling 40 h.

In order to investigate the phase change of the powder after ball milling for 40 h, the powder was analyzed by XRD and the obtained results are shown in Figure 2. In TiH₂-7Al-0.2B powder, after low energy ball milling, TiH₂ takes a small amount of H to form TiH_{1.971}, and the XRD patterns of

TiH₂-7Al-0.2B show the diffraction peaks of TiH_{1.971} and elemental Al. The diffraction peak of B is not observed, because the amount of added B is small and the atomic weight is low. The diffraction peak of elemental Al still exists in the low-energy ball milling process. Al does not form a significant solid solution into the Ti lattice, and also does not react with Ti to form any intermetallic such as TiAl or Ti₃Al. B probably reacts with Ti to form borides during ball milling, but the amount of boride is small, so the XRD is not detected. Similarly, in the case of Ti-7Al-0.2B, only the diffraction peaks of Ti and Al can be detected and no solid solution phenomenon or phase change is observed.

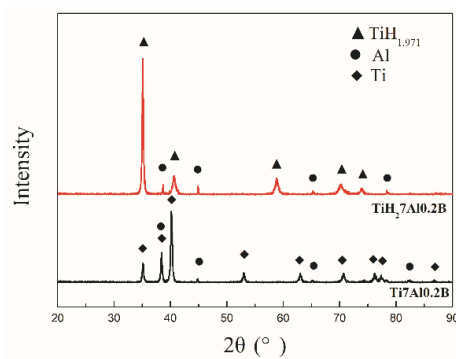


Figure 2. Different components ball milling powder XRD pattern.

3.2. Differential Thermal Analysis

In order to analyze the phase characteristics of the milled powder, two milled powders were subjected to differential scanning calorimetry (DSC, STA 409 PC/PG, NETZSCH, Bavaria, Germany). Figure 3 shows the obtained DSC curves for Ti-7Al-0.2B. An obvious exothermic peak appears at around 660 °C for the ball milling and non-ball milling, which may be due to the phase transition that occurred between Ti and B powders to generate the TiB phase. It can be observed that no endothermic peak appears on the curve. In other words, there is no endothermic phenomenon of Al melting. As the melting point of Al is about 660 °C, it implies that there is no Al existing after the phase change occurred between Ti and B. The phase change temperature of the ball milling powder is slightly lower than that of the non-ball milling powder, and it shows that the reaction between Ti and B more easily occurred after ball milling. The TiH₂-7Al-0.2B test curve is shown in Figure 4. In the temperature range of 450~550 °C, the endothermic peak appears, and TiH₂ is completely decomposed into Ti and H, while a part of the Ti and B phase transformation reaction occurs at about 660 °C to form TiB. According to the DSC analysis, the TiH₂-7Al-0.2B alloy powder dehydrogenation, after ball milling and hot press sintering, caused the reaction to occur between Ti and B to generate TiB phase. The phase composition in the final sintered organization is the same as that of the Ti-7Al-0.2B alloy.

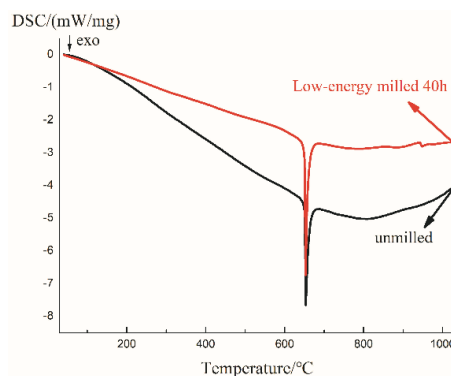


Figure 3. DSC curve of Ti-7Al-0.2B un-milled and low-energy ball milled powders.

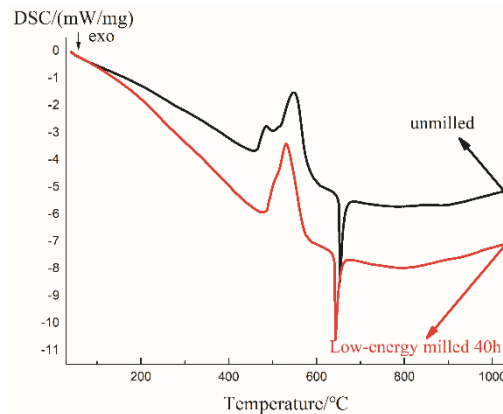


Figure 4. DSC curve of TiH₂-7Al-0.2B un-milled and low-energy ball milled powders.

3.3. Microstructure Analysis

Figure 5 shows the XRD pattern of ball milling powders after sintering. As shown in the picture, both Ti-7Al-0.2B and TiH₂-7Al-0.2B form α -Ti and TiB phase after vacuum hot-pressing sintering. It can be verified that the H in TiH₂-7Al-0.2B powder has no effect on the final sintering microstructure composition due to the dehydrogenation of the powder after sintering. This is in conformity with the phenomena found in the study by Bhosle et al. [16] that the phase transformation of TiH₂ powder in a vacuum environment can be divided into two steps TiH₂ \rightarrow TiH_X (0.7 < X < 1.1) and TiH_X \rightarrow Ti.

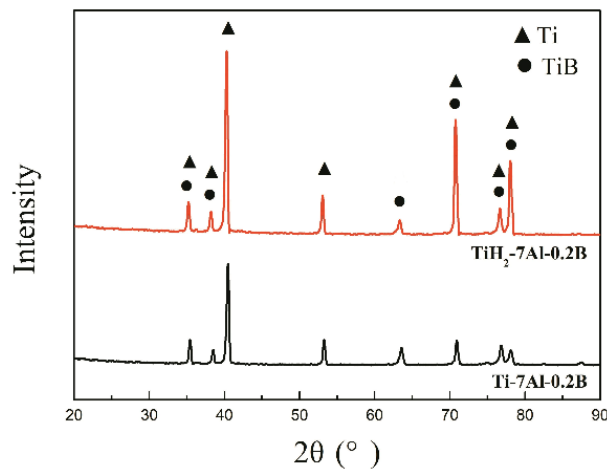


Figure 5. XRD pattern of the sintered alloy.

Figure 6a,b show the SEM images of Ti-7Al-0.2B and TiH₂-7Al-0.2B alloys after sintering. From Figure 6a, it can be seen that the microstructure of sintered Ti-7Al-0.2B alloy is dense, and the TiB reinforcing phase, composed of fine fibers, are uniformly distributed on the α -Ti matrix. In contrast, in Figure 6b there are many residual pores in the microstructure of TiH₂-7Al-0.2B after TiH₂ dehydrogenation [18], and the TiB phase of TiH₂-7Al-0.2B alloy is wilder and shorter than that of the Ti-7Al-0.2B alloy. The grain size of TiH₂-7Al-0.2B alloy is slightly larger than that of Ti-7Al-0.2B alloy, and TiH₂-7Al-0.2B alloy has a grain size between 9 and 44 μ m, and Ti-7Al-0.2B alloy has a grain size between 6 and 25 μ m. This is because the TiB reinforcing phase hinders grain boundary migration and grain growth [19], which makes the TiB phase in Ti-7Al-0.2B alloy finer and more evenly distributed. Figure 6c,d show the energy dispersive spectrometer (EDS) results of Ti-7Al-0.2B and TiH₂-7Al-0.2B alloys after sintering. The chemical compositions of Ti-7Al-0.2B and TiH₂-7Al-0.2B alloys are Ti, Al, and B, which verify that their chemical compositions are the same.

Figure 7 shows the TEM image of the sintered microstructure of Ti-7Al-0.2B alloy. Because the sintered microstructure of TiH₂-7Al-0.2B has some pores, the transmissive samples are easily broken in the process of preparation. TiH₂-7Al-0.2B and Ti-7Al-0.2B alloys have the same components and the same microstructure after the hot-press sintering as discussed earlier, so the morphology shown in Figure 7 can reflect the morphology of these two types of ingredients. From Figure 7a,b, it can be observed that the dislocations are gathered around TiB, and the dislocation density is highest at the boundary. This indicates the reinforcing phase of TiB strongly hinders the dislocation movement in the matrix. The hindering effect of the reinforcing phase on the dislocation is reflected on the improvement of the flow stress of the alloy. A large number of dislocations accumulate at the boundary of the reinforcing phase. When the dislocation density increases to a certain extent, dislocation subgrains are formed. These dislocation subgrains can be used as the core of dynamic recrystallization. In addition, in the deformation process, when the TiB particles rotate in the matrix under the compressive stress, the lattice on both sides of the particle produces a certain phase difference under certain conditions, which can also form subgrains. This subcrystal is also a favorable position for the dynamic recrystallization nucleation. Therefore, in the composite alloys, the hindering effect of the reinforcing phase on dislocation, not only improves the flow stress but also provides favorable conditions for the nucleation and development of dynamic recrystallization. Figure 7c shows the TEM of the net structure. An internal stress is introduced between the powder particles in the process of ball milling, and the internal stress is partially released during the vacuum hot press sintering. The remaining parts form the dislocation structures at grain or grain boundaries. Finally, the dislocation net is formed by dislocation climbing and entanglement.

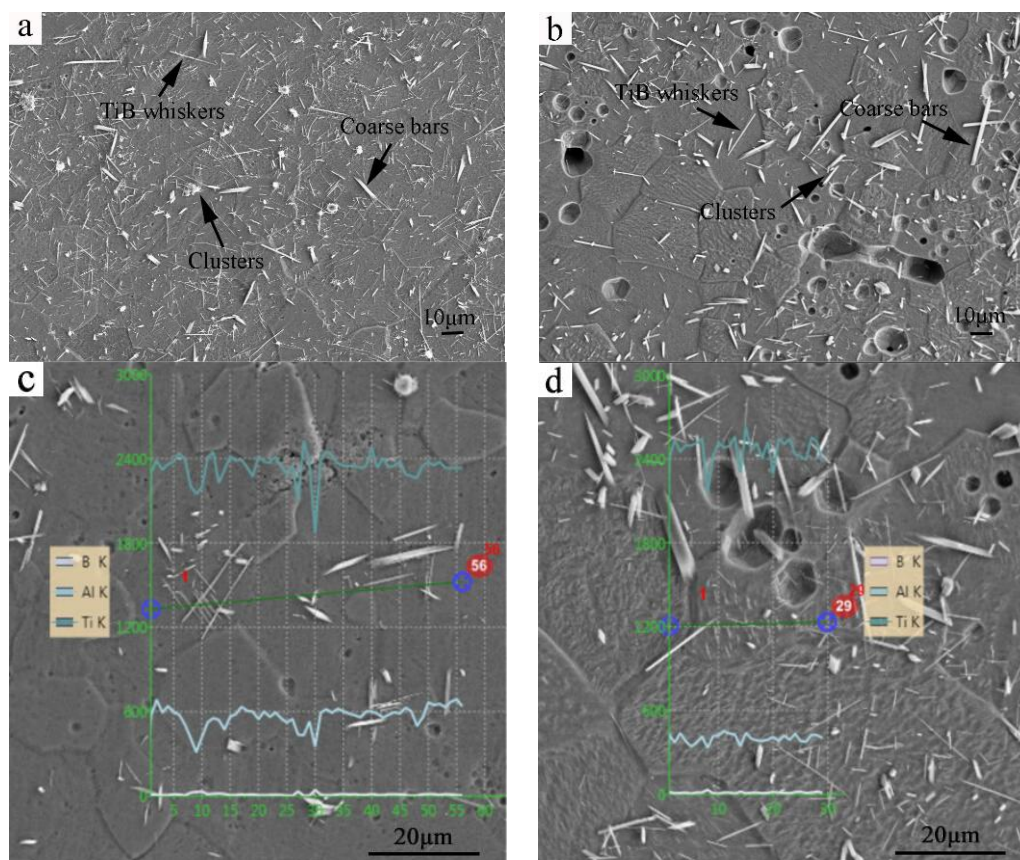


Figure 6. SEM images of sintered alloy: (a) Ti-7Al-0.2B; (b) TiH₂-7Al-0.2B. EDS images of sintered alloy: (c) Ti-7Al-0.2B; (d) TiH₂-7Al-0.2B.

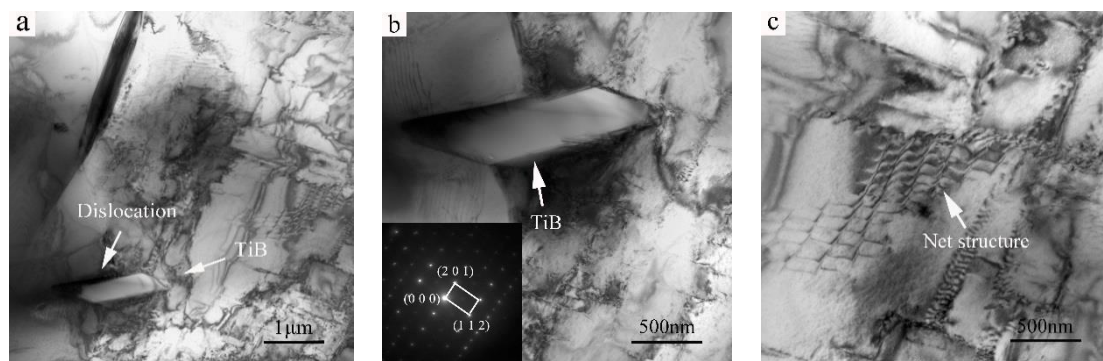


Figure 7. TEM images of Ti-7Al-0.2B, (a) Dislocation, (b) TiB particle and selected area electron microscopy (diffraction pattern), (c) Net structure.

HRTEM analysis of the sample is shown in Figure 8. In Figure 8a, the area of the electron diffraction pattern containing TiB is selected. In Figure 8b, the HRTEM morphology analysis of the selected TiB grain boundaries is shown. The width of the grain boundary between Ti and TiB is 3.84 nm, the interplanar distance of TiB is 0.405 nm, and the angle between the two adjacent interfaces is 57°. The bottom left box area in Figure 8b is the stress field caused by the uniform stress concentration.

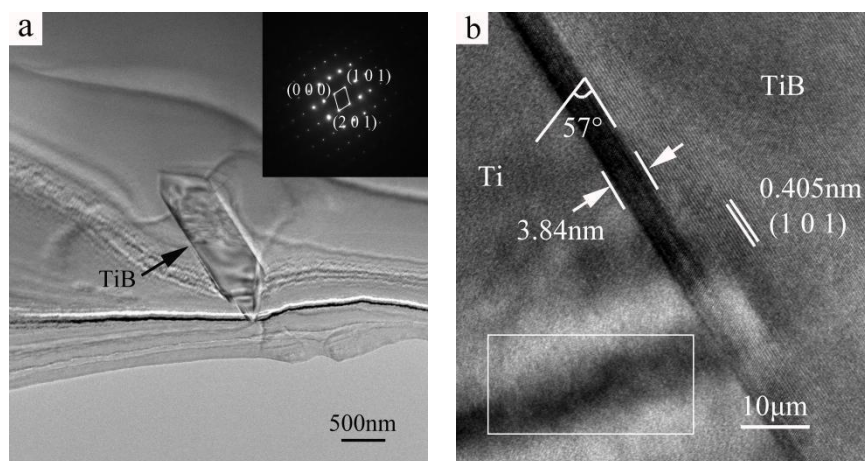


Figure 8. HRTEM morphology of TiB: (a) selected area electron diffraction pattern; (b) TiB grain boundaries.

3.4. True Stress—True Strain Curve Analysis

Ti-7Al-0.2B and TiH₂-7Al-0.2B were compressed into $\Phi 6 \text{ mm} \times 9 \text{ mm}$ samples at the deformation temperatures of 550 °C, 600 °C, and 650 °C. The strain rates are $1 \times 10^{-4} \text{ s}^{-1}$, $3 \times 10^{-4} \text{ s}^{-1}$, and $5 \times 10^{-4} \text{ s}^{-1}$. The deformability of the composite depends on the temperatures of sintering and deformation [20]. An increase in the temperature shows the softening phenomenon of the matrix. In this case, the bearing capacity of the reinforcing phase for load is weakened, and enhancement is also reduced. This can be observed from the compressive yield strength curve, where the slope of the yield strength curve is reduced with the increase in the temperature.

As shown in Figures 9 and 10, the true stress-strain curves of Ti-7Al-0.2B and TiH₂-7Al-0.2B show a similar trend under the same compression conditions. The true stress of the first phase of the experiment begins to increase slowly with an increase in true strain, indicating that there is a dense compressing process of the sample at the beginning of the experiment. The experimental alloys show sensitivity to deformation temperature and strain rate during high-temperature compression.

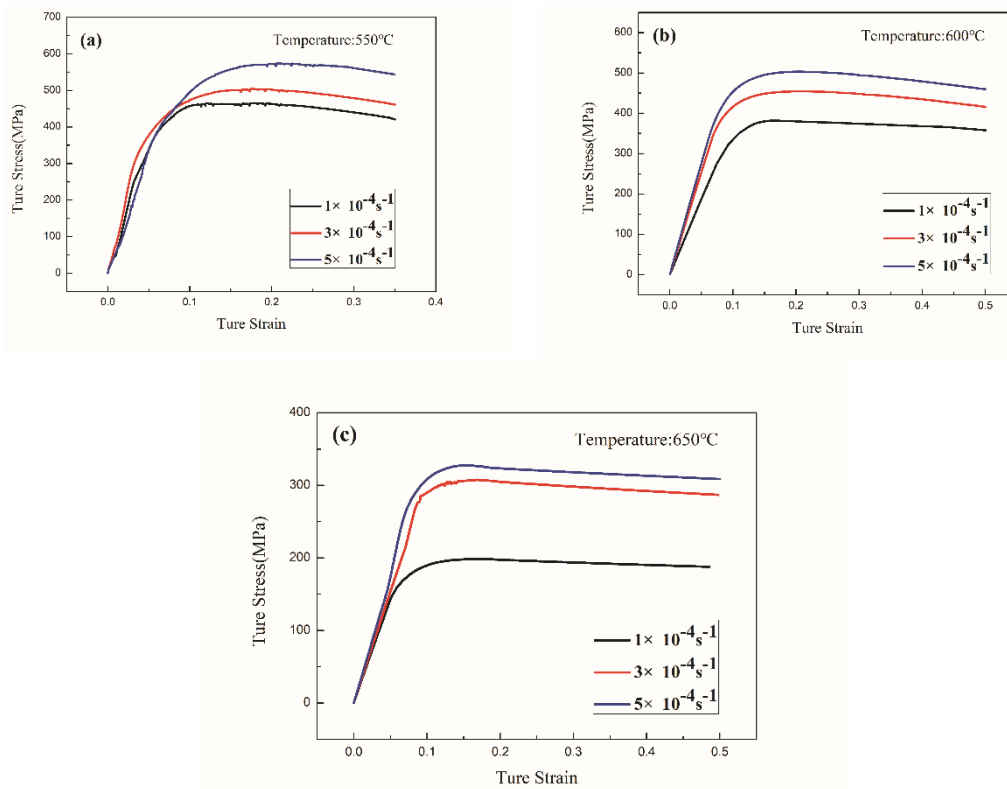


Figure 9. True stress-strain curves of Ti-7Al-0.2B at different temperatures and compressive rates.

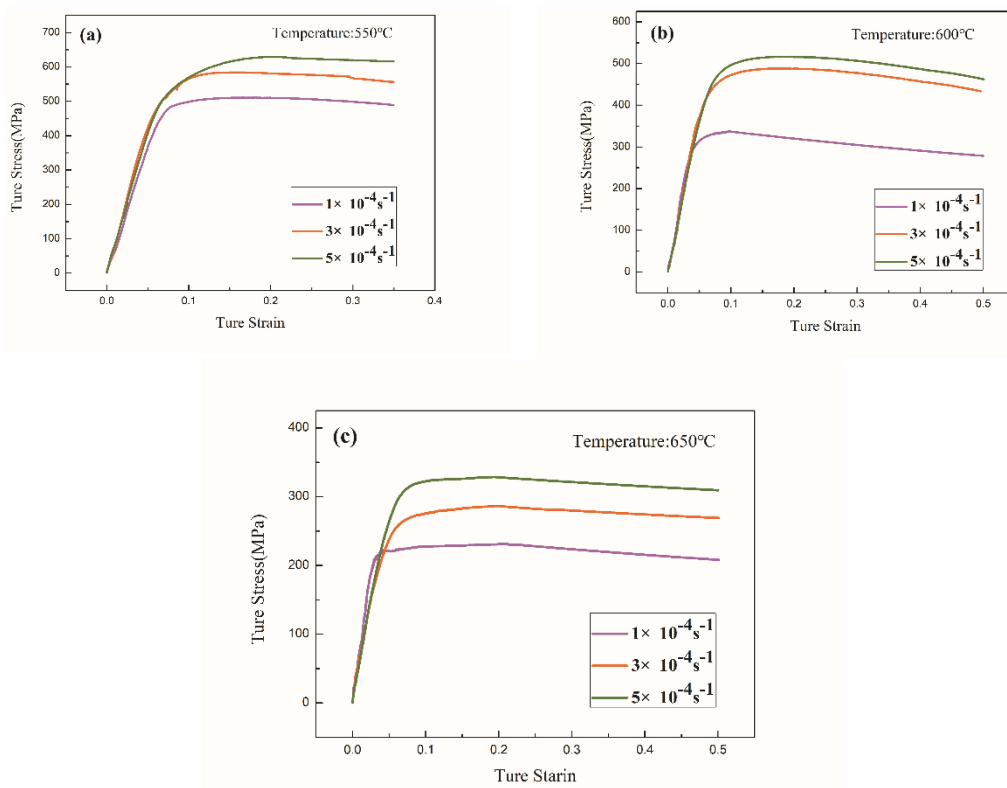


Figure 10. True stress-strain curves of TiH₂-7Al-0.2B at different temperatures and compressive rates.

When the strain rate is constant, the peak of compressive flow stress decreases with an increase in the deformation temperature. Compressing Ti-7Al-0.2B at a rate of $1 \times 10^{-4} \text{ s}^{-1}$, a maximum stress

of 464 MPa is obtained at 550 °C, and a minimum stress of 201 MPa at 650 °C. From compressing TiH₂-7Al-0.2B at a rate of $1 \times 10^{-4} \text{ s}^{-1}$, a maximum stress of 512 MPa is obtained at 550 °C, and a minimum stress rate of 230 MPa at 650 °C.

When the deformation temperature is constant, the peak flow stress increases with the increase of strain rate. From compressing Ti-7Al-0.2B at 550 °C, the maximum stress value of 575 MPa is obtained at the strain rate of $5 \times 10^{-4} \text{ s}^{-1}$, whereas a minimum stress value of 464 MPa is obtained at the strain rate of $1 \times 10^{-4} \text{ s}^{-1}$. Compressing TiH₂-7Al-0.2B at 550 °C, the maximum stress value of 633 MPa is obtained at the strain rate of $5 \times 10^{-4} \text{ s}^{-1}$, whereas the temperature minimum stress value of 512 MPa is obtained at the strain rate of $1 \times 10^{-4} \text{ s}^{-1}$. This is because at lower strain rates, the dislocation accumulation rate is low. At the same time of dislocation accumulation, the softening behaviors such as dislocation glide, dislocation climb, and grain boundary sliding are also weak, resulting in the reduction of work hardening.

Comparing the true stress-strain curves of Ti-7Al-0.2B and TiH₂-7Al-0.2B, it can be observed that the trend, as shown, in the stress-strain curves of these two alloys is consistent. However, at the same temperature and at the same strain rate, the peak flow stress of TiH₂-7Al-0.2B alloy is slightly higher than that of Ti-7Al-0.2B alloy. At the temperature of 550 °C and the strain rate of $5 \times 10^{-4} \text{ s}^{-1}$, where the highest peak flow stress is 575 MPa and 633 MPa for Ti-7Al-0.2B and TiH₂-7Al-0.2B, respectively. This is due to the lower strength of the grain boundary at the high temperature. The intragranular strength increases and the deformation easily starts at the grain boundary. Therefore, the material with fine grains easily begins to deform from the grain boundary at high temperature, but the strength is lower than that of large grains. In addition, in the ball milling and sintering processes of TiH₂-7Al-0.2B, the decomposition of H from TiH₂ cleanses the surface of Ti particles. This leads to the reduction of the possibility of contamination and also has a good effect in improving the compression performance.

4. Conclusions

1. After low-energy ball milling and high-temperature hot-press sintering, Ti-7Al-0.2B and TiH₂-7Al-0.2B alloys were prepared in situ with TiB phase and α -Ti duplex structure. The in situ synthesis of TiB-reinforced phase is advantageous to hinder the migration of grain boundary and grain growth. The TiB phase in Ti-7Al-0.2B alloy is fine and evenly distributed, which shows a strong effect in suppressing the grain growth. Therefore, the grains of Ti-7Al-0.2B alloy are finer between 6 μm and 25 μm , compared to TiH₂-7Al-0.2B alloy. After ball milling and hot-press sintering, TiH₂-7Al-0.2B alloy shows porosity in the sintered structure due to the dehydrogenation process. TiB phase in TiH₂-7Al-0.2B alloy is dominated by the short and coarse strips.
2. Both Ti-7Al-0.2B and TiH₂-7Al-0.2B alloys are heat-sensitive and strain-rate-sensitive. At high-temperature compression, the peak stress decreases with the decrease of the strain rate and the increase of temperature. At the same temperature and at the same strain rate conditions, the maximum peak flow stress of TiH₂-7Al-0.2B is slightly higher than that of Ti-7Al-0.2B. At the temperature of 550 °C and strain rate of $5 \times 10^{-4} \text{ s}^{-1}$, the highest peak flow stress of 631 MPa is obtained, while at the temperature of 650 °C and strain rate of $1 \times 10^{-4} \text{ s}^{-1}$, the peak stress is the lowest 210 MPa. This is due to the decrease in grain boundary strength at high temperature, where the internal strength of the crystal increases and the deformation easily starts at the grain boundary. Therefore, at high temperature, the deformation of fine grain material easily occurs at the grain boundary and the strength of fine grain material is lower than that of larger grains.
3. In the ball milling and sintering process of TiH₂-7Al-0.2B alloy, the decomposition of H from TiH₂ cleanses the surface of Ti particles. This leads to the reduction of the possibility of contamination and also has a good effect in improving the compression performance.

Author Contributions: Jing Zeng and Hua Chen conceived, designed, and wrote the experiments; Liping Liu performed the experiments and analyzed the data; Jiazhi Yuan made the charts and conducted the literature search.

Acknowledgments: The authors would like to thank the National Natural Science Fund (No.51371038) for providing financial support.

Conflicts of Interest: The authors declare no conflict of interest.

References

1. Chandran, K.S.R.; Panda, K.B.; Sahay, S.S. TiB w-reinforced Ti composites: Processing, properties, application prospects, and research needs. *JOM* **2004**, *56*, 42–48. [[CrossRef](#)]
2. Liu, H.X.; Wei, K.X.; Li, J.M.; Zhou, J.Y.; Peng, W.J. Research Progress of Aviation Titanium Alloy. *Trans. Nonferr. Met. Soc. China* **2015**, *25*, 280–292.
3. Wang, X.; Wang, L.; Luo, L.; Xu, Y.; Li, X.; Chen, R.; Su, Y.; Guo, J.; Fu, H. Hydrogen induced softening and hardening for hot workability of (TiB + TiC)/Ti-6Al-4V composites. *Int. J. Hydrog. Energy* **2017**, *42*, 3380–3388. [[CrossRef](#)]
4. Gorsse, S.; Chaminade, J.P.; Petitcorps, Y.L. In situ, preparation of titanium base composites reinforced by TiB single crystals using a powder metallurgy technique. *Compos. A Appl. Sci. Manuf.* **1998**, *29*, 1229–1234. [[CrossRef](#)]
5. Chandran, K.S.R.; Miracle, D.B. Titanium-boron alloys and composites: Processing, properties, and applications. *JOM* **2004**, *56*, 32–33. [[CrossRef](#)]
6. Tjong, S.C.; Ma, Z.Y. Microstructural and mechanical characteristics of in situ metal matrix composites. *Mater. Sci. Eng. R Rep.* **2000**, *29*, 49–113. [[CrossRef](#)]
7. Kim, Y.W. Ordered intermetallic alloys, part III: Gamma titanium aluminides. *JOM* **1994**, *46*, 30–39. [[CrossRef](#)]
8. Abkowitz, S.; Abkowitz, S.M.; Fisher, H.; Schwartz, P.J. CermeTi® discontinuously reinforced Ti-matrix composites: Manufacturing, properties, and applications. *JOM* **2004**, *56*, 37–41. [[CrossRef](#)]
9. Li, X.X. Preparation and Mechanical Properties of In situ Self-Generated (TiC + TiB)/Ti Composites. Master's Thesis, Harbin Institute of Technology, Harbin, China, July 2013.
10. Tang, H.P.; Huang, B.Y.; Liu, Y.; Ouyang, H.W. Progress in the densification of powder metallurgical titanium alloys. *Rare Met. Mater. Eng.* **2003**, *32*, 677–680.
11. Li, B.Y.; Rong, L.J.; Li, Y.Y. The influence of addition of TiH₂, in elemental powder sintering porous Ni-Ti alloys. *Mater. Sci. Eng. A* **2000**, *281*, 169–175. [[CrossRef](#)]
12. Hou, H.L.; Li, Z.Q.; Wang, Y.J.; Guan, Q. Technology of hydrogen treatment for titanium alloy and its application prospect. *Chin. J. Nonferr. Met.* **2003**, *13*, 533–549.
13. Ivasishin, O.M.; Markovsky, P.E.; Semiatin, S.L.; Ward, C.H. Aging response of coarse- and fine-grained β titanium alloys. *Mater. Sci. Eng. A* **2005**, *405*, 296–305. [[CrossRef](#)]
14. Ivasishin, O.M.; Shevchenko, S.V.; Semiatin, S.L. Effect of crystallographic texture on the isothermal beta grain-growth kinetics of Ti-6Al-4V. *Mater. Sci. Eng. A* **2002**, *332*, 343–350. [[CrossRef](#)]
15. Bhosle, V.; Baburaj, E.G.; Miranova, M.; Salama, K. Dehydrogenation of TiH₂. *Mater. Sci. Eng. A* **2003**, *356*, 190–199. [[CrossRef](#)]
16. Zhou, L.; Liu, H.J. Effect of 0.5 wt. % hydrogen addition on microstructural evolution of Ti-6Al-4V alloy in the friction stir welding and post-weld dehydrogenation process. *Mater. Charact.* **2011**, *62*, 1036–1041. [[CrossRef](#)]
17. Cao, Z.Y.; Xiao, P.A.; Lei, B. High-energy planetary ball milling of TiH₂ powder and ultrafine titanium sintering. *TNMSC* **2013**, *10*, 2825–2832.
18. Li, D.R.; Cui, Q.L.; Cai, Y.X. Preparation of TiAl-Based Porous Materials by TiH₂ Foaming and Their Microstructure and Properties. *Powder Metall. Technol.* **2014**, *32*, 96–99.
19. Attar, H.; Ehtemam-Haghighi, S.; Kent, D.; Okulov, I.V.; Wendrock, H.; Bönisch, M.; Volegov, A.S.; Calin, M.; Eckert, J.; Dargusch, M.S. Nanoindentation and wear properties of Ti and Ti-TiB composite materials produced by selective laser melting. *Mater. Sci. Eng. A* **2017**, *688*, 20–26. [[CrossRef](#)]
20. Ozerov, M.; Klimova, M.; Kolesnikov, A.; Stepanov, N.; Zherebtsov, S. Deformation behavior and microstructure evolution of a Ti/TiB metal-matrix composite during high-temperature compression tests. *Mater. Des.* **2016**, *112*, 17–26. [[CrossRef](#)]

